



HAL
open science

3D Semi-Analytical Modeling and Optimization of Fully HTS Ironless Axial Flux Electrical Machines

Yazid Statra, Hocine Menana, Bruno Douine

► **To cite this version:**

Yazid Statra, Hocine Menana, Bruno Douine. 3D Semi-Analytical Modeling and Optimization of Fully HTS Ironless Axial Flux Electrical Machines. *Physica C: Superconductivity and its Applications*, 2020, 574, pp.1353660. 10.1016/j.physc.2020.1353660 . hal-02885281

HAL Id: hal-02885281

<https://hal.science/hal-02885281>

Submitted on 22 Aug 2022

HAL is a multi-disciplinary open access archive for the deposit and dissemination of scientific research documents, whether they are published or not. The documents may come from teaching and research institutions in France or abroad, or from public or private research centers.

L'archive ouverte pluridisciplinaire **HAL**, est destinée au dépôt et à la diffusion de documents scientifiques de niveau recherche, publiés ou non, émanant des établissements d'enseignement et de recherche français ou étrangers, des laboratoires publics ou privés.



Distributed under a Creative Commons Attribution - NonCommercial 4.0 International License

3D Semi-Analytical Modeling and Optimization of Fully HTS Ironless Axial Flux Electrical Machines

Yazid STATRA, Hocine MENANA, Bruno DOUINE
Université de Lorraine, GREEN, F-54000 Nancy, France

Abstract—In this paper, a three-dimensional semi-analytical approach, based on the volume integral method, is developed to compute the forces and torque in fully high temperature superconducting (HTS) ironless axial flux machine (IAFM). The use of particular volumetric basis elements helps to speed up the computation of the magnetic field. The Maxwell stress tensor method is used for the force and torque calculations, where the electromagnetic state of the superconductor is taken into account. The developed model is then introduced into a multi objective optimization procedure, based on the genetic algorithms, to maximize the magnetic torque and minimize the superconducting wire length in the considered structure, while respecting the constraints linked to the physical and mechanical properties of the considered HTS tape. It is shown that the considered fully HTS machine has a higher torque density compared to conventional one.

Keywords—Fully HTS ironless axial flux electrical machine, three-dimensional semi-analytical modeling approach, Volume integral method, Maxwell stress tensor method, Multi objective optimization.

1. INTRODUCTION

Recently, fully high temperature superconducting (HTS) electrical machines have aroused worldwide research efforts due to their high power densities, making them good candidates for embedded applications, such as wind power generation and electrical aircrafts [1-2]. HTS are characterized by high current densities and low power losses, allowing to increase the linear current loading and thus the torque density and the global efficiency of the HTS electrical machines, compared to conventional ones. In addition, the air gap in a fully HTS machine can be made much smaller, compared to hybrid ones (superconducting-copper machines), resulting in a higher magnetic field density [3]. Furthermore, the elimination of the iron core increases the efficiency, due to absence of core losses, and reduces the weight [4]. However, the strong nonlinear behavior of HTS materials makes the sizing and optimization procedures of HTS electrical machines delicate operations, where local electromagnetic quantities have to be evaluated generally in 3D. Numerical approaches are generally inevitable, facing the limitations of conventional numerical tools which struggle in some cases to provide accurate solutions in reasonable computation times, despite the high performances of the recent computers. The development of specific modeling approaches is thus needed to speed up the sizing and optimization procedures of HTS systems. In this context, a volume integral approach is proposed in this work for a rapid 3D modeling of forces and torques in a fully HTS ironless axial flux machine (IAFM). The calculation of the magnetic field using the integral equations is obtained in very short times thanks to the use of particular volumetric basis elements for which the solution is obtained analytically. The developed model is then used in a multi objective optimization, based on genetic algorithms, aiming to maximize the magnetic torque and to minimize the superconducting wire length in the considered structure, respecting the constraints related to the critical bending radius of the superconducting tape and the dependence of the critical current density on the magnetic field. A comparison with 3D finite element analysis on the optimal solution confirms the accuracy and the rapidity of the proposed approach.

The studied HTS-IAFM and the modeling approach are presented in the next section. Section III describe the multi objective optimization procedure. The obtained results for the optimal solution are presented and compared with finite element computation in Section IV. In Section V, a mechanical study is carried out to define the volume of the machine and its torque density, which is then compared to conventional ones.

NOMENCLATURE

μ_0	Vacuum permeability
I_a, I_b, I_c	Current in peak value of a, b, and c phase
I	Current in peak value of the field pole (inductor) coil
B_x, B_y, B_z	Components of the magnetic field in the x, y, and z direction
B_{\perp}, B_{\parallel}	Perpendicular and parallel components of the magnetic field to the large surface of HTS tape
F_z	Axial force
Γ	Static torque
φ	Displacement/ mechanical angle
J	Electric current density
J_c	Critical current density
n	Creep exponent
E	Electric field
E_c	Critical electric field
R_{out}	Outer radius of the machine
R_{int}	Inner radius of the machine
l_w	Coils' thickness, HTS tape's width
e_w	HTS tape's thickness
R_b	Rotor and stator coil's bending radius
R_c	Critical bending radius
e	Thickness of the air gap
k_e	Filling factor of the HTS coils
p	Number of pole pairs
Q	Number of stator coils
α, β	Rotor and stator coils reel opening respectively
L_{sup}	Total superconducting wire length
L_1, L_2	Superconducting wire lengths used in the inductor, armature coils
W_r, W_s	Rotor and stator coil's width respectively
N_r, N_s	Rotor and stator coil's number of turns respectively
$V = [p \ x_1 \ x_2 \ x_3]$	Vector of the optimization variables

2. THE MODELLING APPROACH

The structure of the studied HTS-IAFM is shown in Fig.1. It consists of an axial flux synchronous machine constituted of two sets of triangular shaped HTS coils mounted on nonmagnetic supports. The structure parameters are given in Table I. The inductor coils are supplied by DC currents I in a way to obtain alternatively north and south poles. This is the rotating part of the machine. The stator with three-phase double-layer concentrated nonoverlapping armature windings is supplied by AC currents. The use of concentrated nonoverlapping coils has certain advantages: shorter end-turn length and reduced stator winding cost due to the reduced number of coils and the simplicity of the winding [5-6]. This choice is more appropriate when using HTS materials, where it is necessary to take into account the limitations of the HTS related to the critical current and bend radius. The ironless windings are fixed on the anterior sides of epoxy resin supports (G11) containing guide-track grooves for coils embedding, as shown in Fig. 1(a).

A magneto-static modeling of the machine is performed. The aim is to evaluate the forces and torque between the two set of coils, taking into account the dependence of the critical current density in the HTS coils on the magnetic field. The Biot-Savart's law is used to compute the magnetic field produced by the HTS coils. The three-phase windings are fed with electrical current such as $I_a = I$ and $I_b = I_c = -I/2$ corresponding to AC operation at a given instant of the time variation of the three phase currents. As shown in Fig. 1(b), the coils are discretized into rectangular beam or circular arc segment volume elements of rectangular cross sections. The magnetic field created by the structure is then the superposition of the magnetic fields created by the basic elements. Figure 1(c) gives more details on the rotor coils dimensions and orientation.

2.1. Magnetic field calculation

Let (x, y, z) be a field point and in Cartesian coordinates system; then, the magnetic flux density for a straight beam with rectangular cross section, parallel to the z axis, with a cross section $(x_2-x_1) \times (y_2-y_1)$, length (z_2-z_1) , carrying a constant current density J oriented in the positive z direction, is given as follows [7]:

$$B_m(x, y, z) = \frac{\mu_0 J}{4\pi} \sum_{i,j,k=1}^2 (-1)^{i+j+k} A_m(x, y, z) \quad m = x, y \quad (1)$$

$$\begin{cases} A_x(x, y, z) = -u_i \sinh^{-1} \theta_1 - w_k \sinh^{-1} \theta_2 + v_j \tanh^{-1} \theta_5, \\ A_y(x, y, z) = v_j \sinh^{-1} \theta_1 + w_k \sinh^{-1} \theta_3 - u_i \tanh^{-1} \theta_4, \end{cases} \quad (2)$$

Where:

$$\begin{aligned} u_i &= x_i - x, v_j = y_j - y, w_k = z_k - z \\ \alpha_{ij}^2 &= u_i^2 + v_j^2, \beta_{jk}^2 = v_j^2 + w_k^2, \gamma_{ki}^2 = w_k^2 + u_i^2, \\ r^2 &= u_i^2 + v_j^2 + w_k^2, \theta_1 = w_k / \alpha_{ij}, \theta_2 = u_i / \beta_{jk}, \theta_3 = v_j / \gamma_{ki}, \\ \theta_4 &= v_j w_k / u_i r, \theta_5 = u_i w_k / v_j r \quad i, j, k = 1, 2, \end{aligned} \quad (3)$$

The expressions of the components of the magnetic field for a circular arc segment are also available in [7]. However,

in this work, we use the expressions given by (Eq. 4) which are simpler to implement [8]. Indeed, in this case, the analytical integration of the Biot-Savart's law was performed along two coordinates, obtaining a 1-D integrand (thus avoiding the use of elliptic integrals). The result is very satisfying in terms of rapidity and precision.

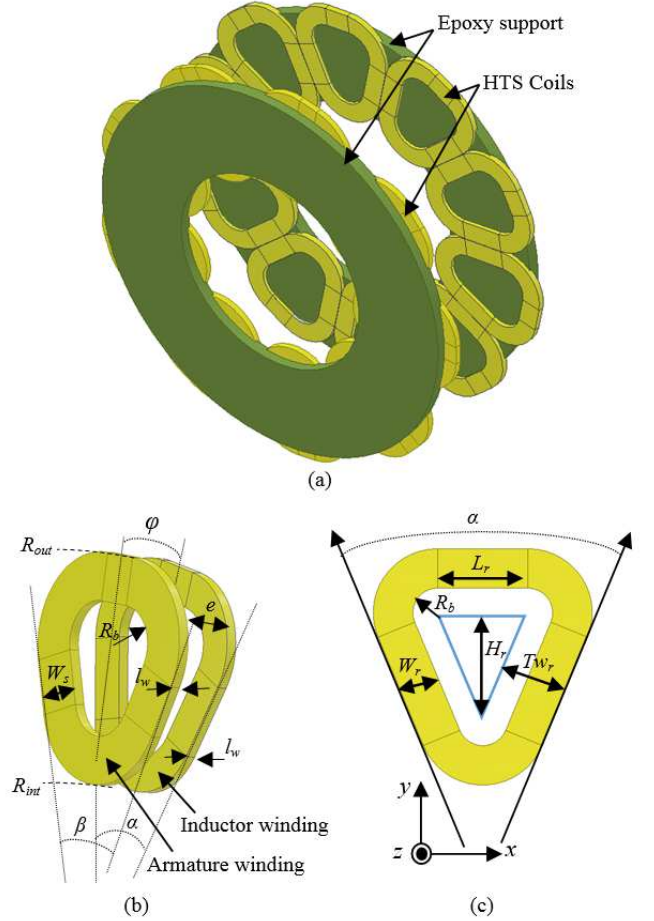


Fig. 1. Geometry of the modelled HTS ironless axial flux machine ($p=5$, $Q=9$) (a) Topology (b) Coils structure and dimensions (c) details on the rotor coils dimensions and orientation

TABLE I. PARAMETERS OF THE STUDIED HTS-IAFM

Parameter	Description	Value
R_{out}	Outer radius	350 mm
l_w	Coils thickness	4.3 mm
e	Thickness of the air gap	5 mm
k_e	Filling factor	0.83

$$\begin{aligned} B_x(x, y, z) &= \frac{\mu_0 J}{4\pi} \int_{\varphi_1}^{\varphi_2} L_{xy} \cos(\varphi) d\varphi \\ B_y(x, y, z) &= -\frac{\mu_0 J}{4\pi} \int_{\varphi_1}^{\varphi_2} L_{xy} \sin(\varphi) d\varphi \\ B_z(x, y, z) &= \frac{\mu_0 J}{4\pi} \int_{\varphi_1}^{\varphi_2} (L_z + 0.5T_1 \cdot \ln(M) + f \cdot R_A) d\varphi \end{aligned} \quad (4)$$

The analytical expressions of L_{xy} , L_z , T_1 , M , f and R_A depend directly on the geometrical parameters of the studied structure [8].

2.2. Force and torque calculations

The axial force (F_z) and the static torque (Γ) are obtained by the integration of the Maxwell stress tensor on a surface (S) located in the middle of the air gap between the two sets of coils:

$$F_z = \frac{1}{\mu_0} \iint_S \frac{1}{2} (B_z^2 - B_x^2 - B_y^2) dx dy \quad (5)$$

$$\Gamma = -\frac{1}{\mu_0} \iint_S (B_y B_z x - B_x B_z y) dx dy \quad (6)$$

2.3. Operating current of the HTS coils

The critical current density of a superconducting coil does not only depend on the temperature, but also on the applied magnetic field. The increase of the magnetic field lead to a decrease of the critical current density, and thus the degradation of the HTS material performances. Indeed, superconducting materials have a nonlinear behavior represented by (7), where E and E_c are the electrical field and its critical value respectively; J and J_c are the electric current density and its critical value respectively, and n is the creep exponent that defines the steepness of the transition from the superconducting to the normal state. The critical current density and the creep exponent depend on both the temperature and the magnetic field.

$$E = E_c \left(\frac{J}{J_c(B)} \right)^{n(B)} \quad (7)$$

The considered HTS coils are assumed to be made of 1G BSCOO tape. In such material, the critical current density and the creep exponent exhibit an anisotropic dependence on the magnetic field, which can be modelled by the Kim's model, given by (8), where J_{c0} and n_0 are the values of the critical current density and the creep exponent at zero magnetic field [9].

$$\begin{cases} J_c(B_{\perp}, B_{//}) = \frac{J_{c0}}{\left(1 + B_{j0}^{-1} \sqrt{k^2 B_{//}^2 + B_{\perp}^2}\right)^{\delta}} \\ n(B_{\perp}, B_{//}) = \frac{n_0}{\left(1 + B_{n0}^{-1} \sqrt{k^2 B_{//}^2 + B_{\perp}^2}\right)} \end{cases} \quad (8)$$

The width and thickness of the used BSCCO tape are respectively: $l_w = 4.3 \text{ mm}$ and $e_w = 0.23 \text{ mm}$. The critical bending radius of the tape is: $R_c = 35 \text{ mm}$. Its main characteristics at 30 K are listed in Table II [10].

TABLE II. CHARACTERISTICS OF THE HTS TAPE @ 30K

Parameter	J_{c0}	B_{j0}	k	δ	n_0	B_{n0}
Value	537 A/mm ²	1.01 T	0.182	0.87	31	2 T

The critical value of the electric field is usually set to: $E_c = 1 \mu\text{V/cm}$ [9-10]. The operating current is obtained for a maximum value of the electric field applied locally on the

coil that is equal to E_c , i.e. $\max(E/E_c) = 1$. This requires some iterations using (7) and (8). The current is increased as long as $\max(E/E_c) < 1$. However, in the optimization procedure this takes a lot of time. Therefore, an alternative method to calculate the operating current is adopted: the operating current is obtained by the intersection between the load line representing the current as a function of the maximum magnetic field applied locally on the coil and the curves $I_c(B_{\perp}, B_{//})$. This method provides a faster estimation of the operating current. Indeed, obtaining the load line requires the knowledge of only one operating point of the coil.

3. MULTI OBJECTIVES OPTIMIZATION

The developed semi-analytical model is used in a multi objective optimization procedure based on the Non-Dominated Sorting Genetic Algorithm (NSGA II) [11]. The goal is to maximize the magnetic torque (Eq.6), and to minimize the superconducting wire length (L_{sup}) which is the sum of L_1 and L_2 , where:

$$L_1 = \left(\frac{H_r}{\cos(\alpha/2)} + \frac{L_r}{2} + \frac{\pi(2T_{w_r} - W_r)}{2} \right) 4p N_r \quad (9)$$

$$L_2 = \left(\frac{H_s}{\cos(\beta/2)} + \frac{L_s}{2} + \frac{\pi(2T_{w_s} - W_s)}{2} \right) 2Q N_s \quad (10)$$

In (9) and (10), Q is the number of stator coils, while N_s and N_r represent the number of turn in a coil of the stator and the rotor respectively. The other parameters are given by the following equations:

$$\alpha = \frac{\pi}{p} \quad (11)$$

$$\beta = \frac{2\pi}{Q} \quad (12)$$

$$T_{w_s} = \frac{R_{int} \sin(\beta/2)}{1 - \sin(\beta/2)} \quad (13)$$

$$T_{w_r} = \frac{R_{int} \sin(\alpha/2)}{1 - \sin(\alpha/2)} \quad (14)$$

$$H_s = R_{out} - R_{int} - 2 * T_{w_s} \quad (15)$$

$$H_r = R_{out} - R_{int} - 2 * T_{w_r} \quad (16)$$

$$L_s = 2H_s \tan(\beta/2) \quad (17)$$

$$L_r = 2H_r \tan(\alpha/2) \quad (18)$$

$$N_s = [W_s K_e / e_w] \quad (19)$$

$$N_r = [W_r K_e / e_w] \quad (20)$$

The optimization variables are given in table III. The optimization procedure consists to determine the vector $V = [p \ x_1 \ x_2 \ x_3]$ of optimal variables that verify the objective functions, respecting the constraints related to bending radius given in table IV and critical current density. To avoid local transition and quench in the HTS coils, especially in the armature windings (working at low frequencies), only 80% of the critical current is injected in the HTS coils.

TABLE III. RANGE OF VARIATION OF THE OPTIMISATION VARIABLES

Parameter	Description	Range	Nature
p	Number of pole pairs	[2-8]	Integer
$x_1 = R_{int}/R_{out}$	Coefficient which defines the inner radius	[0.1-0.6]	Real
$x_2 = W_s/TW_s$	Coefficient which defines the stator coil's width	[0.1-0.6]	Real
$x_3 = W_r/TW_r$	Coefficient which defines the rotor coil's width	[0.1-0.7]	Real

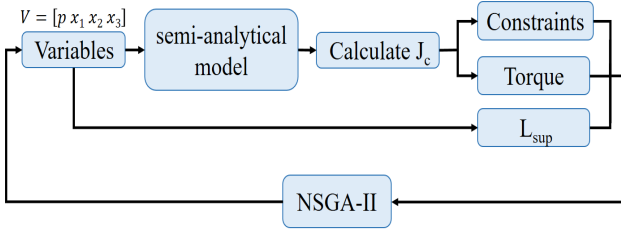
TABLE IV. CONSTRAINTS ON THE OPTIMISATION VARIABLES

Parameter	Min Value	Max Value
x_1	$Max \left\{ \begin{array}{l} \frac{(R_c + 2e_w)(1 - \sin(\alpha/2))}{R_{out} \sin(\alpha/2)} \\ \frac{(R_c + 2e_w)(1 - \sin(\beta/2))}{R_{out} \sin(\beta/2)} \end{array} \right\}$	$Min \left\{ \begin{array}{l} \left(1 + \frac{2\sin(\alpha/2)}{1 - \sin(\alpha/2)}\right)^{-1} \\ \left(1 + \frac{2\sin(\beta/2)}{1 - \sin(\beta/2)}\right)^{-1} \end{array} \right\}$
x_2	$2e_w/TW_s$	$1 - R_c/TW_s$
x_3	$2e_w/TW_r$	$1 - R_c/TW_r$

The block diagram shown in Fig. 2 presents the general structure of the optimization procedure, in which the main steps are:

- i. Definition and insertion of the vector of the optimization variables in the semi-analytical model.
- ii. Evaluation the superconducting wire length $L_{sup} = L_1 + L_2$.
- iii. Evaluation the critical current density J_c for the position ($\varphi = 0^\circ$), corresponding to the worst case.
- iv. For $J = 80\% J_c$, determine the maximum value of the torque corresponding to the displacement angle $\varphi = \pi/(2p)$.

The algorithm verifies the objective functions and satisfies the imposed constraints by repeating the steps i-iv.

**Fig. 2.** Process of the optimization

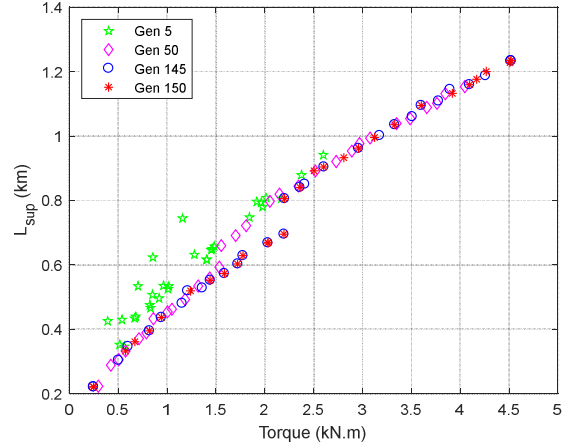
4. RESULTS

The algorithm gives possible compromises between the two criteria (torque and superconducting wire length) as shown in Fig.3 which represent the evolution of the Pareto front according to the number of generations for a population of 30 individuals. These compromises strongly depend on the constraints imposed. We notice that the algorithm converges after 145 generations.

The configuration for which the couple is maximum in Fig.3 is selected. The values of the corresponding optimization variables are given in Table V. The results of the torque and the axial forces calculated by the semi-analytical model have then been compared with 3D finite element analysis performed on COMSOL software [12], in the aim of validation. A formulation in terms of the magnetic vector potential is used in the 3D FEM.

Figures 4 and 5 show, respectively, the axial force and the static torque as a function of the mechanical rotor position φ . The axial force reaches a maximum value of 23.5 kN for $\varphi = 0^\circ$, while the torque has a maximum value of 4.52 kN.m for $\varphi = 18^\circ$. We also notice that the axial force has no mean value due to the absence of ferromagnetic materials in the studied structure. The axial force and static torque calculated with the proposed approach are in good accordance with those obtained by 3D FEM simulation. However, for one point of computation, the computing time is in the order of few seconds using the proposed approach, while it is around ten minutes for the FEM.

Figure 6 shows a comparison between semi-analytical and finite element calculations of the operating current density of the superconducting coils for $\varphi = 0^\circ$, which corresponds to the worst case, by using the maximum electric field criterion: $\max(E/E_c) = 1$. The obtained critical current density is about 268 A/mm^2 . It can be seen that the results of the semi-analytical model are close to those obtained by the finite elements analysis. The difference between the analytical and numerical calculations of the operating current density, for both methods described above (section 2.3), is less than 0.4 % as shown in table VI.

**Fig. 3.** Evolution of the Pareto front according to the number of generations**TABLE V.** PARAMETERS OF THE HTS-IAFM AFTER OPTIMIZATION

Parameter	Description	Value
p	Number of pole pairs	5
R_{in}	Inner radius	149 mm
W_r	Rotor coil's width	42.26 mm
W_s	Stator coil's width	31.5 mm
Γ	Torque value	4.52 kN.m
L_{sup}	Superconducting wire length	1.23 km
J_c	Critical current density	268.22 A/mm ²

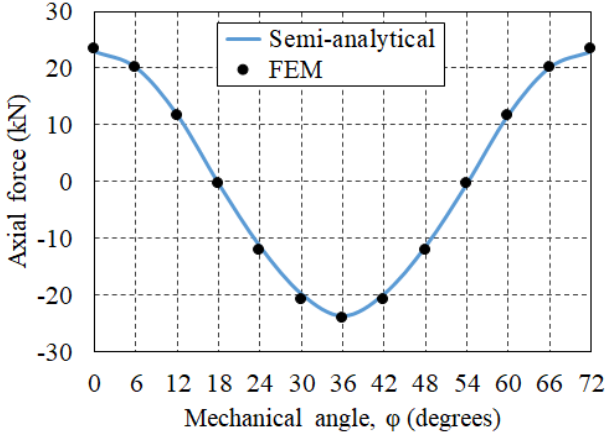


Fig. 4. Axial force versus mechanical rotor position (ϕ)

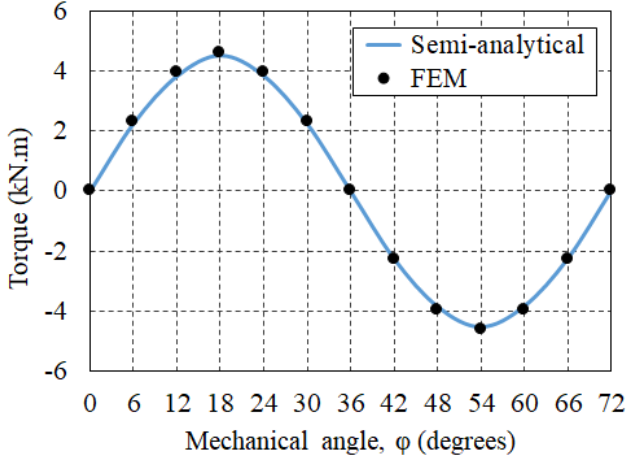


Fig. 5. Static torque versus mechanical rotor position (ϕ)

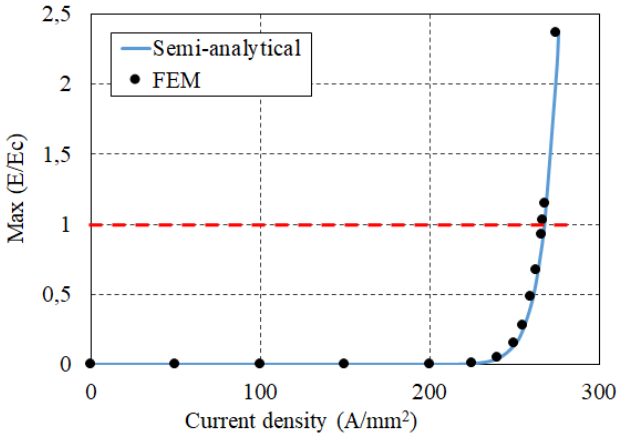


Fig. 6. Operating current of the superconducting coils according to the criterion on the maximum electric field for $\phi = 0$.

TABLE VI. RESULTS OF THE OPERATING CURRENT DENSITY

J_c (A/mm ²)	Max(E/E_c)	Load line	Difference
Semi-analytical	268	267.9	0.037 %
FEM	267	267.36	0.135 %
Difference	0.37 %	0.2 %	

5. MECHANICAL STUDY

This part aims to estimate the thickness of the mechanical supports of the two sets of HTS coils in order to resist to the axial forces. As already mentioned above, the coils are placed on supports made from G11 material. This kind of support ensures the thermal insulation between the superconducting coils and the motor shaft which is at the room temperature. Figure 7 (a) shows the shape of the support structure. It has an inner and outer diameter of 56mm and 740mm respectively. The inner diameter which represent the diameter of the motor shaft is calculated using the following relation [13]:

$$D \geq \left(\frac{16\Gamma}{\pi\tau} \right)^{\frac{1}{3}} \quad (19)$$

Where, τ and Γ represent, respectively, the maximum shear stress and the torque supported by the shaft. Using a safety factor of two, the diameter is calculated to be able to transmit twice the maximum torque calculated previously with the maximum stress equal to the half of the tensile strength of the steel used to make the shaft (565 MPa) [14].

The volume axial forces obtained for a position ($\phi=0^\circ$) on COMSOL software, are illustrated in Fig. 7(b). It can be seen that these forces are not applied equally on all the coils. The force is greater in the coils of phase (a). Indeed, the latter is supplied by a current I , while the other phases are supplied by currents equal to $\pm I/2$.

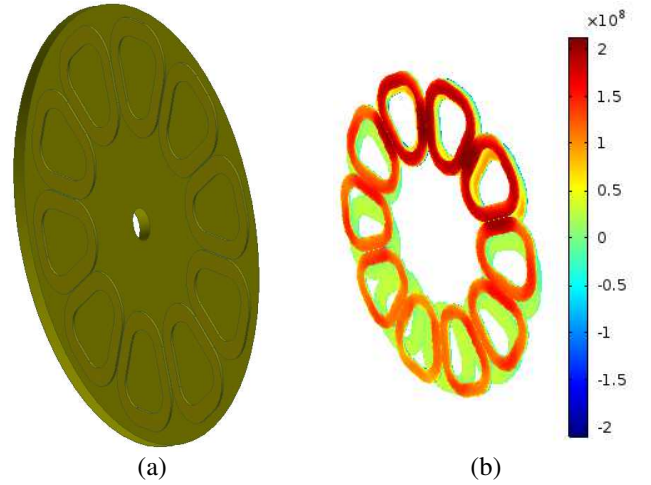


Fig. 7. (a) Support structure (b) Volume axial force distribution (N/m^3)

To evaluate the maximum stress applied on the supports, the worst case is considered:

- By integrating the greatest force applied on one coil, we find an axial force of 6300 N.
- We applied on the two set of coils a total force of 63 kN which represents the force applied to a coil multiplied by the maximum number of coils in one set (10 in this case).

The distribution of the stress applied to one of the supports for a thickness of 30 mm, is represented in Fig. 8. It can be

noticed that the highest stress occurs on the surface close to the motor shaft, where fixed constraint is applied. Figure 9 shows the evolution of the maximum stress applied locally on the support and the displacement between the two supports as a function of the support thickness. The thickness of the mechanical support is chosen so that the displacement and the stress do not exceed 10% the thickness of the air gap, and the half of the tensile strength of the used material (Von Mises Criteria) respectively (Table VII). The result is a thickness of 35 mm, leading to an approximate torque density of the machine of 156 kN/m^3 , which is much higher than that of conventional machines [15]. This result takes into account only the volume of the active parts.

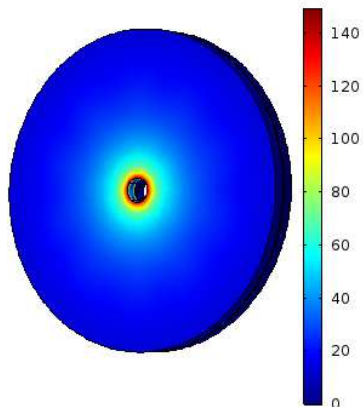


Fig. 8. The distribution of the stress en MPa for a thickness of 30 mm.

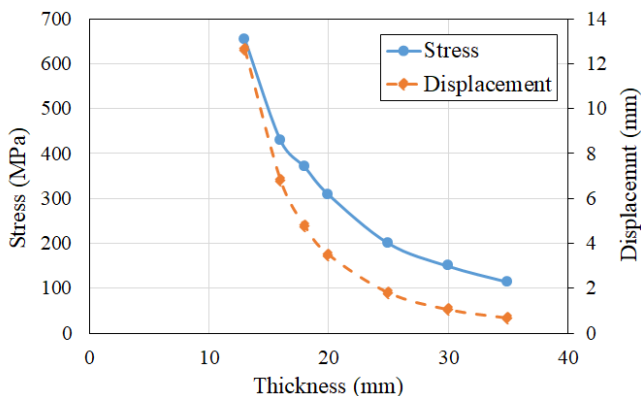


Fig. 9. Maximum stress and displacement versus the thickness of the support.

TABLE VII. EXTRAPOLATED MECHANICAL PROPERTIES OF THE USED MATERIAL [14]

G11-CR	Young's Modulus (E) (GPa)	Poisson's ratio, ν	tensile strength (MPa)
Temperature : (30 K)	102.53	0.216	856

6. CONCLUSION

The design and optimization of superconducting electrical machines is mainly based on the evaluation of local quantities, due to the strong dependence of superconductive material performances to the magnetic

field, and rapid modeling approaches are needed. In this context, this paper presents a three-dimensional semi-analytical approach based on the volume integral method for the forces and torque calculations in a fully HTS ironless axial flux synchronous machine. The performances of the developed model and its advantages, compared to 3D FEM analysis, have been shown on a multi-objective optimization example. The considered example allowed also to appreciate the performances of the fully HTS electrical machines compared to conventional ones. The evaluation of AC losses in the HTS coils, and the cryogenic system sizing will be studied in future work.

REFERENCES

- [1] M. Ainslie et al, Recent advances in superconducting rotating machines: an introduction to the 'Focus on Superconducting Rotating Machines', *Supercond. Sci. Technol.*, 29(6) (April 2016) 060303.
- [2] M. Zhang, F. Eastham and W. Yuan, Design and Modeling of 2G HTS Armature Winding for Electric Aircraft Propulsion Applications, *IEEE Trans. Appl. Superconduct.*, 26(3) (April 2016) 1-5.
- [3] D. Dezhin, N. Ivanov, K. Kovalev, I. Kobzeva and V. Semehin, System Approach of Usability of HTS Electrical Machines in Future Electric Aircraft, *IEEE Trans. Appl. Superconduct.*, 28(4) (June 2018) 1-5.
- [4] R. Ravaut, G. Lemarquand and V. Lemarquand, Ironless permanent magnet motors: Three-dimensional analytical calculation, *2009 IEEE International Electric Machines and Drives Conference*, Miami, FL, (2009) 947-952.
- [5] W. Geng and Z. Zhang, Analysis and Implementation of New Ironless Stator Axial-Flux Permanent Magnet Machine With Concentrated Nonoverlapping Windings, *IEEE Trans. on Energy Conversion*, 33(3) (Sept. 2018) 1274-1284.
- [6] M. J. Kamper, R. Wang and F. G. Rossouw, Analysis and Performance of Axial Flux Permanent-Magnet Machine With Air-Cored Nonoverlapping Concentrated Stator Windings, *IEEE Trans. on Industry Applications*, 44(5) (Sept.-Oct. 2008) 1495-1504.
- [7] L. Urankar, Vector potential and magnetic field of current-carrying finite arc segment in analytical form, Part III: Exact computation for rectangular cross section, *IEEE Trans. Magn.*, 18(6) (November 1982) 1860-1867.
- [8] A. Capelluto, M. Nervi and P. Molino, Algorithm for the Fast Calculation of Magnetic Fields Generated by Arc-Shaped Conductors With Rectangular Cross Section, *IEEE Trans. Appl. Superconduct.*, 24(6) (Dec. 2014) 1-5.
- [9] Y. Statra, H. Menana, L. Belguerras and B. Douine, A volume integral approach for the modelling and design of HTS coils, *COMPEL- The international journal for computation and mathematics in electrical and electronic engineering*, 38(4) (July 2019) 1133-1140. <https://doi.org/10.1108/COMPEL-10-2018-0392>.
- [10] L. Belguerras, L. Hadjout, S. Mezani, T. Lubin and A. Rezzoug, Study of HTS Magnetic Coupler Using Analytical and Numerical Computations, *IEEE Transactions on Applied Superconductivity*, 24(6) (Dec. 2014) 1-12.
- [11] K. Deb, A. Pratap, S. Agarwal et T. Meyarivan, A Fast and Elitist Multiobjective Genetic Algorithm: NSGA-II, *IEEE Transactions on Evolutionary Computation*, 6(2) (2002) 182-197.
- [12] Comsol, Finit-element software package comsol multiphysic version 4.2 (2011). available at: www.comsol.com
- [13] Jean-Louis Fanchon, Guide de mécanique, Nathan, (2001) ISBN 978-2-09-178965-1.
- [14] Carl L. Goodzeit, SUPERCONDUCTING ACCELERATOR MAGNETS: An Introduction to Mechanical Design and Construction Methods, USPAS, (January 2001).
- [15] M. Dubois, H. Polinder, et J. A. Ferreira, Comparison of generator topologies for direct-drive wind turbines, *In : Proceedings of IEEE Nordic Workshop on Power and Industrial Electronics*, Aalborg, Denmark, (Norpie 2000) 22-26.